Inorganic Chemistry

pubs.acs.org/IC Article

Influence of Number of Ligands and Point Group on the Electronic Structure of Co^{2+} Aqua-Complexes

Liesbeth De Bruecker and Veronique Van Speybroeck*

Cite This: *Inorg. Chem.* 2022, 61, 20743−20756 Read Online

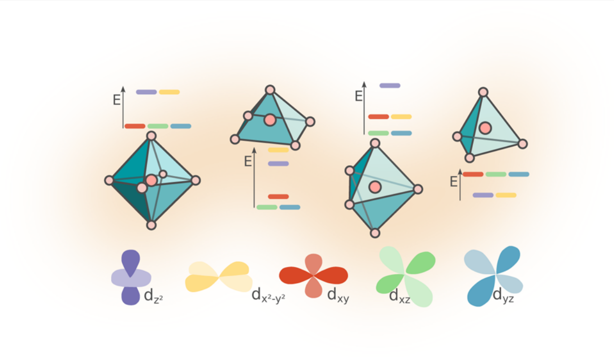

ABSTRACT: The nucleation process of zeolitic imidazolate frameworks (ZIFs) is, to date, not yet completely understood, making the search for tailored materials very difficult. Recently, it has been shown that, during the formation process, the symmetry of the precursors is reduced by ligand elimination and substitution reactions. The octahedral precursors with simple ligands, such as water, methanol, and/or NO_3^-, are transformed to five- and finally four-coordinated complexes with imidazole ligands. This reduction of symmetry, caused both by the changing coordination environment and distortions from the perfect symmetry leading to another point group, will have a large influence on the electronic structure and more specifically on the d-orbital splitting. This, in turn, will affect the d−d electronic excitations, which can be followed using UV−vis spectroscopy and which can help to unravel the formation process. In this work, we systematically investigate how the lowering of the number of ligands affects the symmetry and thus the geometry and electronic structure of Co^{2+} complexes with six, five, and four aqua ligands. Therefore, we first resort to qualitative techniques, such as crystal field theory (CFT) and ligand field theory (LFT), which reveal that the orbital splitting is characteristic for the number of ligands. However, as these techniques are not capable of providing quantitative results without the use of experimental data as input, we perform various computational calculations. Both average of configuration (AOC) and unrestricted density functional theory (UDFT) are thoroughly investigated, and we will determine which technique is the best suited to properly describe the ground state of these systems. To investigate the dependency on the d-orbital occupation, we also investigated V^{2+}, Mn^{2+}, and Ni^{2+} hexa-aqua-complexes and compared them to the Co systems.

1. INTRODUCTION

Zeolitic imidazolate frameworks (ZIFs) are a subclass of metal−organic frameworks (MOFs) in which divalent metal cations, mostly Fe^{2+}, Co^{2+}, Cu^{2+}, or Zn^{2+}, are tetrahedrally coordinated by bridging imidazolate-type linkers.[1−6] Since the cation-linker-cation angle in ZIFs is similar to the Si−O−Si angle in zeolites, they are topologically isomorphic, hence their name.[1,7−9] ZIFs are due to their chemical stability, robust porosity, and resistance to thermal changes very promising candidate materials for several applications. Among others, we mention the use as catalysts or carbon dioxide caption materials,[10] molecular sieves for gas separation,[11] and high-impact shock absorbers.[12] Zn-ZIF-8 is a typical model system, consisting of tetrahedrally coordinated Zn^{2+} ions bridged by 2-methylimidazolate (2-mIm).[1,3,5,13−15] By replacing the Zn^{2+} cations with Co^{2+}, the iso-structural Co-ZIF-67 is obtained,[16−19] which has a sodalite topology and $Co(2\text{-}mIm)_4^{2-}$ tetrahedral secondary building units (SBUs), as shown in Figure 1.

An in-depth understanding of the formation process of these materials is indispensable for a targeted search for structures with the best properties for a specific application, as this is at the moment mainly done *via* high-throughput synthesis.[21] Although the particle nucleation step is more or less understood by now,[22,23] the underlying molecular assembly processes in the pre-nucleation stage have been less thoroughly investigated and remain largely unknown. Only very recently, a combined experimental−computational study has been conducted,[24] in which it is suggested that, during Co-ZIF-67 nucleation, a metal−organic pool with a variety of complexes is formed caused by ligand elimination and substitution reactions. This is visualized with green and blue arrows, respectively, in Figure 2. In this way, the symmetry of the octahedral precursors in methanol solution, $[CoL_6]^{2+}$, with L simple ligands like aqua, methanol, and/or NO_3^-, is lowered by two mechanisms during the nucleation process. On the one hand, some of the ligands are substituted with imidazole; on the other hand, some of them are eliminated. The complex

Received: July 7, 2022
Published: December 15, 2022

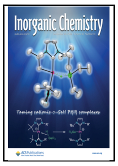

https://doi.org/10.1021/acs.inorgchem.2c02358
Inorg. Chem. 2022, 61, 20743−20756

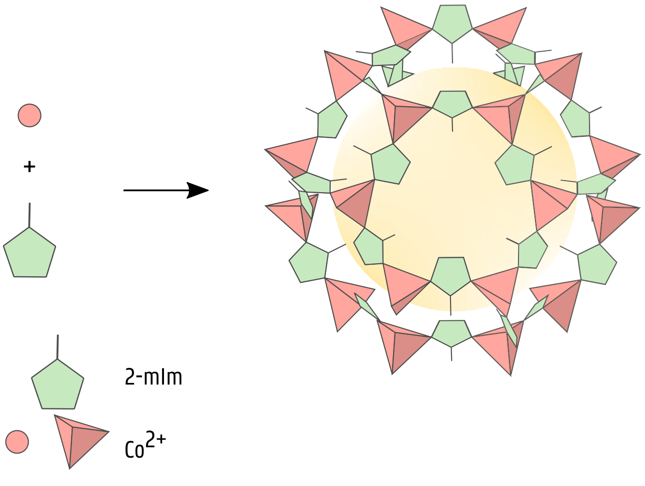

Figure 1. Crystal structure of Co-ZIF-67. Co^{2+} is indicated with a circle when it is isolated and with a tetrahedron when coordinated with the 2-mIm linkers. Figure adapted from ref 20 with permission of Elsevier, 2015.

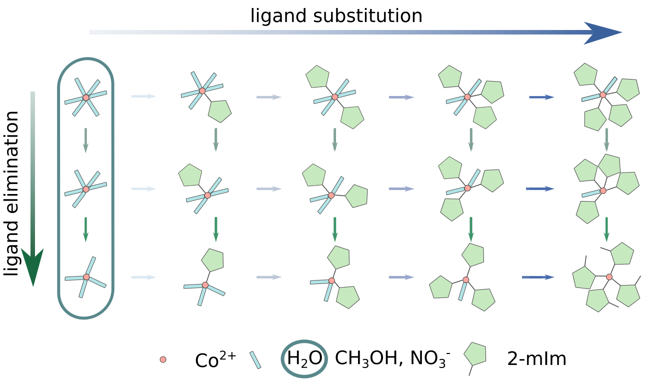

Figure 2. Reaction network of ligand elimination and substitution reactions leading to fast preequilibrium formation toward a metal–organic pool. Co^{2+} complexes with six, five, and four aqua ligands are studied in this work and are indicated. Figure adapted from ref 24 with permission of Elsevier, 2021.

thus goes from $[CoL_6]^{2+}$, an octahedral system with six simple ligands, over a five-coordinated system, toward $Co(2\text{-mIm})_4^{2-}$, a tetrahedral complex with four 2-mIm ligands, which are the building blocks of Co-ZIF-67. To fully understand this complicated mechanism, we would like to follow the evolution of the UV–vis spectrum, and more specifically, of the d–d transitions, as the number of them and the intensity with which they occur change during the course of the formation process and can therefore serve as a fingerprint for the crystal formation process. An excellent recent review on computational molecular spectroscopy can be found in ref 25.

In this work, we investigate six-coordinated octahedral, five-coordinated square pyramidal (SP), five-coordinated trigonal bipyramidal (TBP), and four-coordinated tetrahedral Co^{2+} complexes, as shown in Figure 2. We restrict ourselves to aqua ligands as, in particular for hexa-aqua Co^{2+} complexes, we can compare our results to previous studies. We will concentrate on the ground-state properties as they need to be described correctly and understood completely before an investigation of the excited states can be started. The ground-state properties of TMCs still pose various challenges as for example recently shown in refs 26 and 27 for the calculation of spin-state energetics.

As stated before, octahedral Co^{2+} aqua-complexes have already been extensively studied in the literature. Structural properties and excitation energies have been obtained from experimental studies.[28−33] Besides this, $[Co(H_2O)_6]^{2+}$ has also been the subject of many computational investigations as it can serve as a model system for much more complicated Co^{2+} complexes, and, due to its small size, direct comparisons to highly correlated *ab initio* calculations are feasible.[34] A detailed review of the ground-state properties using a wide variety of computational methods has been given in ref 35. More recent works also investigate the excited states but this lies outside the scope of this work.[36−39] These complexes have also already been investigated using multireference *ab initio* calculations where solvent effects have been included.[40]

In the present study, we will extend the computational results by examining the electronic structure of these complexes, and more specifically, we will focus on the influence of symmetry on the position of the energy levels of the d-orbitals as this is decisive for the d–d transitions. There are two origins for the changes in symmetry. First of all, large influences are expected when the number of ligands is changed, resulting in various coordination environments, *i.e.*, octahedral,

Table 1. Overview of the Complexes Studied in This Work, Ordered Based on Their Number of Aqua Ligands[a]

Number of aqua ligands	Symmetry	Visualisation of geometry	Elements studied
6	Octahedral	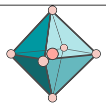	Co^{2+}, V^{2+}, Mn^{2+}, Ni^{2+}
5	Square pyramidal (SP)	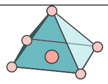	Co^{2+}
	Trigonal bipyramidal (TBP)	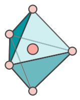	Co^{2+}
4	Tetrahedral	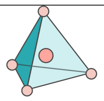	Co^{2+}

[a]For every system, both AOC and UDFT calculations are performed. Experimental data are available for the six-coordinated complexes.

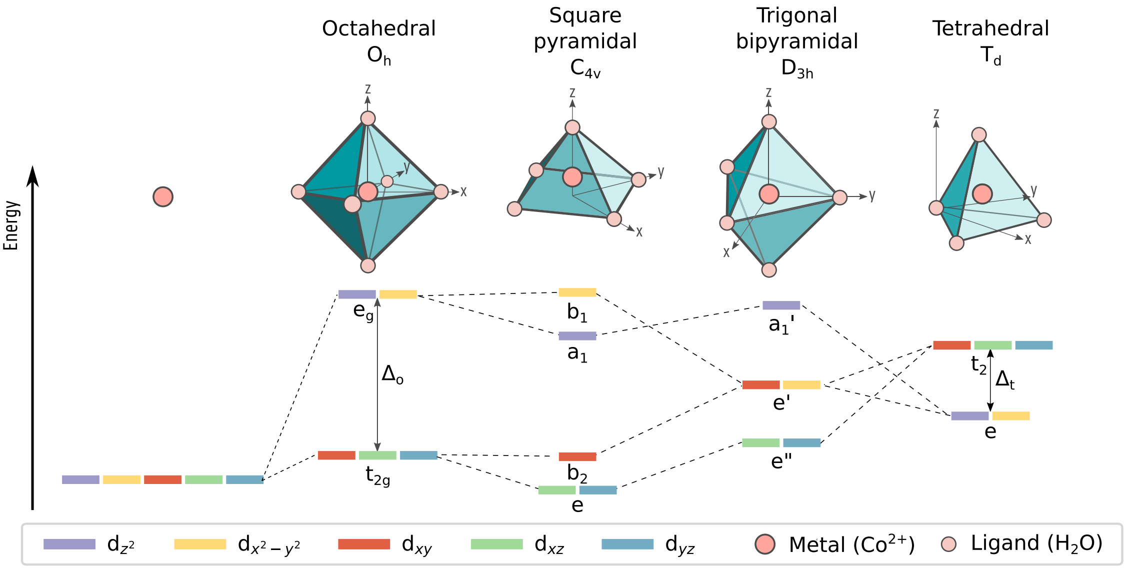

Figure 3. Splitting of the d-orbitals for a TM in various environments. For an isolated TM, all d-orbitals are degenerate, whereas for complexes with octahedral, SP, TBP, and tetrahedral symmetry, the degeneracy is (partially) lifted. The splitting between the two orbital sets in octahedral and tetrahedral complexes is denoted by Δ_o and Δ_t, respectively. The labeling of the d-orbitals in the various point groups is also indicated.

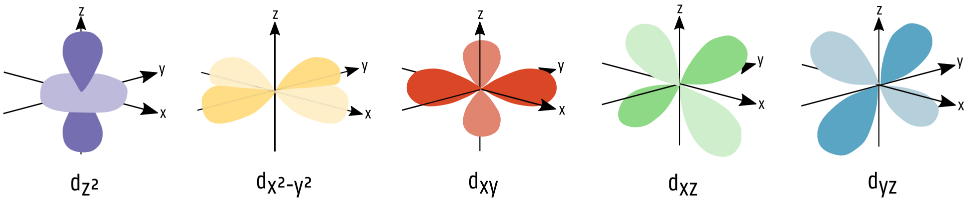

Figure 4. Graphical visualization of the five d-orbitals: d_{z^2}, $d_{x^2-y^2}$, d_{xy}, d_{xz}, and d_{yz}.

SP, TBP, and tetrahedral. Furthermore, additional effects will be studied for the various point groups encountered for each coordination environment as we will note that deviations from the perfect symmetry are present. We will search for, and find, stable structures which are capable of reproducing the experimental data. Furthermore, we will explore how the properties of these complexes change when one and two of the aqua ligands are removed and how this reduction in symmetry is translated in alternations of the d-orbital splitting. To validate our results, we will make comparisons with experimental data where possible.

The remainder of this work is organized as follows. First, we focus on the qualitative predictions for the d-orbital splitting in various coordination symmetries obtained from theoretical techniques such as crystal field theory (CFT), ligand field theory (LFT), and the angular overlap method (AOM). In the next section, the results from density functional theory (DFT) calculations, both average of configuration (AOC) and unrestricted density functional theory (UDFT), are discussed. The molecular orbitals (MOs) with large contributions from d-orbitals will be studied in-depth and more particular, we will concentrate on the influence of symmetry on the splitting of these orbitals. We will determine which technique is suited to correctly describe the ground-state properties of these transitions metal complexes (TMCs). Besides Co^{2+}, we will also investigate other transition metals, V^{2+}, Mn^{2+}, and Ni^{2+}, the d-orbital splitting of which poses less challenges, as will be explained in Section 3.6. In the final section, we conclude with the main outcomes obtained in this study. An overview of the systems studied in this work is given in Table 1.

2. QUALITATIVE INSIGHTS INTO THE D-ORBITAL SPLITTING *VIA* CFT, LFT, AND AOM

In the past century, several theoretical models have been introduced to describe the electronic structure of TMCs, which are still extensively used. First, Becke and Van Vleck applied the CFT, which already existed for the description of metal ions in crystals, to isolated TMCs.[41−43] In this electrostatic approach, ligands are approximated by point charges. The metal d-orbitals pointing toward the ligands will raise in energy due to electrostatic repulsion, whereas the d-orbitals directed between the ligands remain relatively unaffected. As such, this approach predicts the d-orbital splittings in coordination complexes with various symmetries. However, as this method does not describe metal−ligand bonding, LFT, combining CFT and molecular orbital theory (MOT), has been introduced by Griffith and Orgel.[44] It describes the interactions between metal and ligand frontier orbitals which are responsible for the formation of MOs. Additionally, the AOM takes into account the angular geometry of the complex and estimates the strength of interaction between individual ligand orbitals and metal d-orbitals based on their mutual overlap.[45,46] The benefit of this technique is that it is capable of treating systems with little or no symmetry. This comes at the cost of the large number of parameters to be determined from experiment.[47] These models present different approaches to solve the electronic structure of TMCs and all have their advantages and disadvantages, but in general, they give the same qualitative results. These methods can be made quantitative by determining the parameters from experimental absorption spectra. However, we will not focus on this and only give a qualitative explanation of the results as shown in Figure 3 for complexes with various symmetries.

For an isolated TM ion, all five d-orbitals are degenerate, *i.e.*, d_{z^2}, $d_{x^2-y^2}$, d_{xy}, d_{xz}, and d_{yz}, indicated in purple, yellow, red, green, and blue, respectively, and have the same energy. A graphical visualization of these orbitals is shown in Figure 4. Two of them, *i.e.*, d_{z^2} and $d_{x^2-y^2}$, have lobes that are oriented along the coordinate axes, whereas the lobes of the other orbitals are situated in between the coordinate axes. As will be discussed later, the orientation plays an important role when coordinating with ligands. When the TM atom is surrounded by ligands, the average energy of the five d-orbitals is above that of the free ion orbitals because of the electrostatic field generated by the ligands. Furthermore, the degeneracy of the d-orbitals is (partially) lifted. This will be studied in the subsequent paragraphs for six-, five-, and four-coordinated complexes.

Octahedral complexes have six ligands positioned along the coordinate axes and situated at the corners of an octahedron with the TM in the center, as shown in Figure 3. The degeneracy of the d-orbitals is raised partially as they split in two degenerate orbital sets: t_{2g} and e_g; d_{z^2} and $d_{x^2-y^2}$ with lobes directed toward the ligands are raised in energy by the electrostatic repulsion between the electrons of the TM and the ligands and form the e_g set. The t_{2g} set contains d_{xy}, d_{xz}, and d_{yz}, with lobes oriented in between the ligands, and therefore, they remain relatively unaffected. The energy gap between these two sets is indicated in Figure 3 by Δ_o, where the subscript o denotes that this is the splitting for octahedral complexes. When we assume that the ligands are spherical symmetric, the corresponding symmetry is octahedral, O_h. However, as will be seen later, the symmetry will be lowered for aqua ligands.

When removing one ligand, a distinction needs to be made between the removal of a ligand oriented along the *z*-direction or one lying in the *xy*-plane. When one of the ligands along the *z*-direction is eliminated, the SP structure, which belongs to the C_{4v} point group, is obtained; d_{z^2}, d_{xz}, and d_{yz} are stabilized, compared to the octahedral case, as the repulsive interaction between the orbitals and one of the ligands on the *z*-axis is now no longer present. When one of the ligands in the *xy*-plane is removed, the TBP structure, belonging to D_{3h}, is retrieved. As opposed to the octahedral complex, d_{xy} and $d_{x^2-y^2}$ are increased/decreased in energy, respectively, because they point more/less toward the ligands. The application of the AOM shows that the overall splitting of the *d*-orbitals is smaller in D_{3h} than in C_{4v} symmetry.[48] The labeling of the orbital sets in these point groups is indicated in Figure 3.

When, starting from the TBP structure, another ligand is taken out along the *z*-axis, we obtain a tetrahedral structure with T_d symmetry, in which the ligands are situated in between the coordinate axes and at the origin. In contrast to the octahedral complex, d_{xy}, d_{xz}, and d_{yz}, grouped in t_2, now point toward the ligands, whereas $d_{x^2-y^2}$ and d_{z^2}, forming the *e* set, are situated in between the ligands. Therefore, the *e* set is more stable in comparison with the t_2 set. In a similar way as for the octahedral complexes, we can define Δ_t, the splitting between the t_{2g} and e_g orbitals. Δ_t is smaller compared to the octahedral case since the ligands are not oriented directly toward the d-orbitals and therefore the effects will be smaller. This is in agreement with AOM calculations, which show that $\Delta_t \approx \frac{4}{9}\Delta_o$ [49].

These d-orbital splittings are in accordance with the LFT results of Solomon et al.,[50] who studied six-, five-, and four-coordinated Fe^{2+} complexes with oxygen-type ligands.

As stated before, quantitative d-orbital splittings can be obtained from techniques such as LFT using experimental input data. However herein, we will perform computational calculations based on DFT to acquire quantitative d-orbital splittings for Co^{2+} aqua-complexes, as will be discussed in Section 3. As a consequence, we will perform computational calculations to obtain qualitative results for Co^{2+} aqua-complexes, as will be discussed in Section 3. These *ab initio* results can then be compared to the theoretical predictions shown in Figure 3 and to the available experimental information.

3. QUANTITATIVE *AB INITIO* CALCULATIONS: AOC AND UDFT

In this section, the computational techniques used to study Co^{2+} complexes with six, five, and four aqua ligands are explained. The results are analyzed and compared to the qualitative outcomes shown in Figure 3. Before diving into this, attention is paid to the different spin multiplicities Co^{2+} ions can possess.

The Co^{2+} ion has seven d-electrons, which can be placed in five d-orbitals. There are two possible spin multiplicities, 4 and 2, forming the high-spin (HS) and low-spin (LS) configurations, respectively. In the former, as much as possible electrons are unpaired, whereas in the latter, only 1 unpaired electron is present. According to the spectrochemical series, water is a weak ligand.[51] Therefore, Δ_o in octahedral complexes is rather small and the energy needed to pair two electrons is larger than the energy required to place an electron in the higher-lying e_g set. Hence, the HS state of $[Co(H_2O)_6]^{2+}$ is more stable, resulting in five *α*- and two *β*-electrons. This is also in agreement with the DFT study on relative stabilities reported in ref 52. Moreover, since $\Delta_t < \Delta_o$, we can conclude that the HS configuration of the tetrahedral complex will also be more stable than the LS state. Finally, it has also been observed that, in five-coordinated complexes, ligands with oxygen donor atoms usually result in HS configurations.[53,54]

In this work, two types of calculations have been performed, AOC and UDFT, both based on DFT. In AOC, a spin-restricted self-consistent field (SCF) DFT calculation of the d^7 configuration is performed, in which the d-electrons are distributed evenly among the five MOs dominated by d-orbitals. This results in an average occupation of 1.4 electrons. One thus allows systems with fractional occupation numbers. Indeed, one of the great advantages of DFT is, as it is based on the electron density, that there is no formal constraint that orbitals must have integer occupations.[55] Remark that the spin multiplicity is not imposed in these calculations. Meanwhile, in UDFT, the spin multiplicity is specified and all of the five *α*-orbitals are filled, whereas only two *β*-orbitals are occupied.

In the following, the AOC results are discussed in detail for $[Co(H_2O)_6]^{2+}$, $[Co(H_2O)_5]^{2+}$, and $[Co(H_2O)_4]^{2+}$. We systematically investigate how the lowering of the number of ligands affects the symmetry and thus the geometry and electronic structure of these Co^{2+} complexes. This is followed by a comparison between AOC and UDFT. As outlined in the

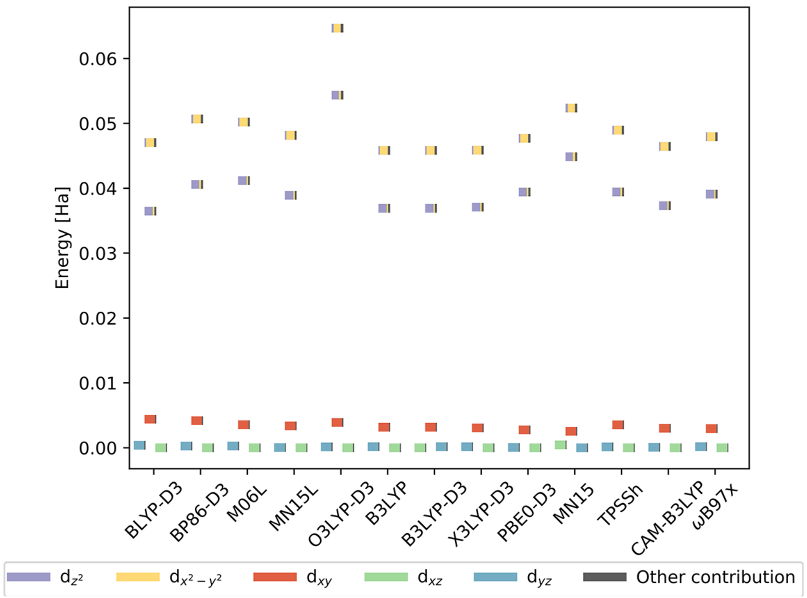

Figure 5. Splitting of the d-orbitals along with their atomic contributions for $[Co(H_2O)_6]^{2+}$ with D_{2h} symmetry obtained from AOC calculations. Different functionals have been used for the geometry optimizations as displayed on the horizontal axis. For the AOC calculations, Grimme D3 dispersion corrections have not been included since they only affect the geometry but not the orbital energies. Energies are shifted with respect to the lowest d-orbital.

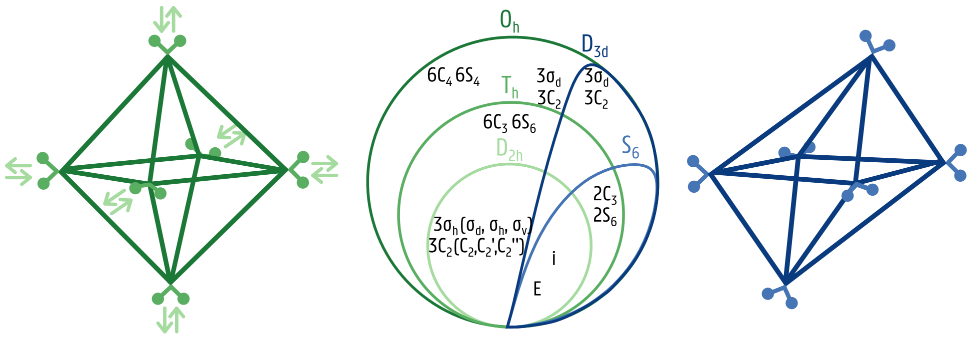

Figure 6. Graphical visualization of the point groups encountered for the six-coordinated complexes, *i.e.*, O_h, T_h, D_{2h}, D_{3d}, and S_6. In the middle pane, all symmetry elements enclosed belong to the corresponding point group. Perfect octahedral symmetry, O_h is indicated in dark green. The presence of hydrogen atoms reduces the symmetry to T_h and is indicated in middle green. Elongation or contraction of the metal−ligand bonds results in D_{2h} symmetry and is shown in light green. An increase or decrease of the ligand−metal−ligand angles leads to a tilted structure with D_{3d} symmetry and is presented in dark blue. When the hydrogen atoms are taken into account in the tilted structure, the S_6 symmetry is obtained as shown in light blue.

Section 3.1, optimized structures have been obtained using UDFT.

3.1. Computational Details. The calculations, both AOC and UDFT, were performed with the Amsterdam modeling suite (AMS).[56] The TZ2P+ basis set, with extra d-Slater type orbitals (STO), has been applied for the transition metals, and the TZ2P basis set has been used for the other elements. Methanol has been included as a solvent using COSMO.[57] Radoń et al. recently revealed that the inclusion of the second solvation shell is important to properly determine the exited states of octahedral aqua-complexes.[40] However, for the aqua-complexes studied in this work, the environment is more complex and consists of both water and methanol to mimic the experimental conditions valid in the formation of ZIFs. A full study of the influence of the complex solvation environment on the chemical and electronic properties of the aqua-complexes is beyond the scope of this article since here we focus on the influence of reducing the number of aqua ligands directly coordinated to the transition metal. Scalar relativistic effects were taken into account using the ZORA formalism.[58−60] Grimme D3 dispersion corrections, which affect the geometry but not the orbital energies, have also been added.[61] We have made use of several functionals coming from different rungs on Jacob's ladder to test their performance in reproducing the d-orbital splitting of $[Co(H_2O)_6]^{2+}$ with D_{2h} symmetry, which will be explained in Section 3.2, using AOC calculations. We assessed the following functionals: BLYP[62] and BP86[63] based on the generalized gradient approximation (GGA), M06L[64] and MN15L[65] built on the meta GGA (mGGA), O3LYP,[66] B3LYP,[62,67] X3LYP,[68] PBE0,[69] and MN15[70] as hybrid GGA, with 12, 20, 21.8, 25, and 44% of Hartree−Fock exchange, the hybrid mGGA TPSSh[71,72] with 10% Hartree−Fock exchange, and the long-range corrected CAM-B3LYP[73] and ωB97x.[74] The results are shown in Figure 5. It stands immediately out that not enough Hartree−Fock exchange is included in O3LYP, for which the splitting between the e_g and t_{2g} set is too large. All other functionals have similar results. We have chosen to continue with B3LYP-D3.

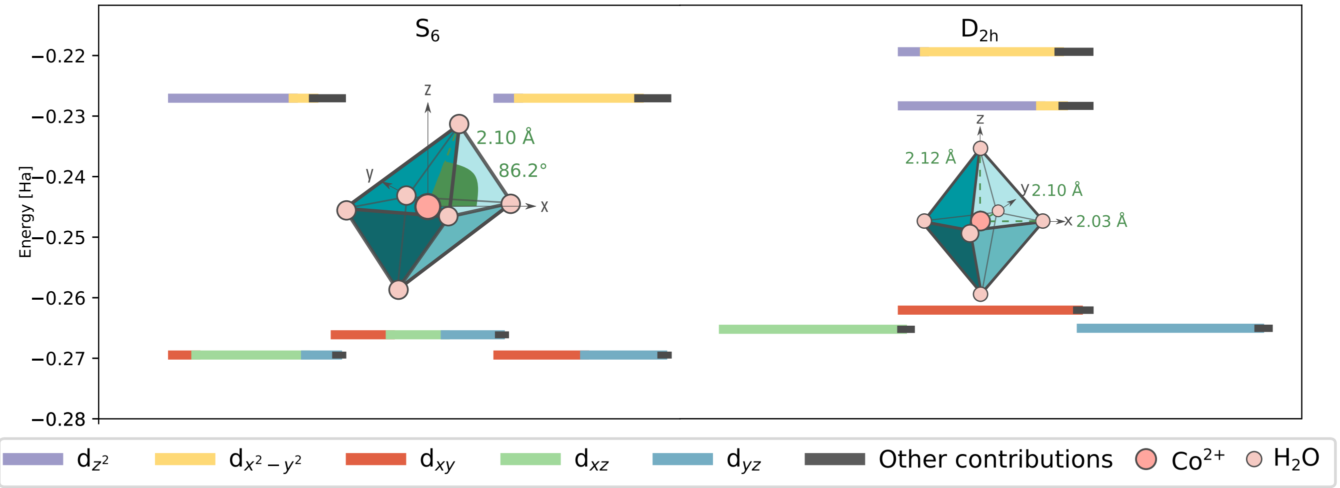

Figure 7. Splitting of the d-orbitals along with their atomic contributions for the optimized $[Co(H_2O)_6]^{2+}$ complexes with S_6 (left) and D_{2h} (right) symmetry. Some bond lengths [Å] and bond angles [deg] are also indicated.

Geometry optimizations have been performed using UDFT. We checked that all computed internal normal modes of the optimized structures show positive frequencies, ensuring that the geometries represent minima of the ground-state potential energy surface. The optimized coordinates of all complexes studied in this work are shown in Table S6. The spin contamination is negligible for all systems as shown in Table S1. The symmetry of the complexes has been determined by GaussView 5.0.[75]

Using the single-reference UDFT method for these challenging electronic structure systems may at first instance appear to be unsatisfactory. However, Shee et al. have recently put forward that in most transition-metal complexes, static correlation is rarely found in the ground states of mono-TMCs.[76] Furthermore, it has been shown that often good structures and energies are obtained from DFT calculations at a moderate computational cost.[77] Hence, we chose DFT to describe the ground-state properties of these systems. Nevertheless, as there are complex interactions present, including ligand-to-metal σ-donation and metal-to-ligand π-backdonation, proper treatment of the dynamic correlation becomes extremely important.

3.2. AOC: $[Co(H_2O)_6]^{2+}$. Octahedral TMCs belong to the O_h point group when the ligands have spherical symmetry. However, when we take into account the structure of the aqua ligands, the highest possible symmetry becomes T_h, with six equivalent ligand bond distances and all O−Co−O angles equal to 90 or 180°. A graphical visualization of the symmetry elements present in the point groups encountered for $[Co(H_2O)_6]^{2+}$ is presented in Figure 6. The geometrical structure of $[Co(H_2O)_6]^{2+}$ has already been investigated thoroughly in the literature. DFT studies have been performed by both Varadwaj et al.[35] and Schmiedekamp et al.[52] Calculations have been performed at the following levels of theory, respectively: UX3LYP and UB3LYP with a 6-311++G** full core basis set and B3LYP with LACVP** effective core potential basis set for Co and 6-31G** basis for all other atoms. Varadwaj et al. compared their results with 163 structures containing the $[Co(H_2O)_6]^{2+}$ ion found in the Cambridge structural database (CSD).[78] Most of the structures, 122 out of the 163 found in the CSD, have three different pairs of bond lengths, the shortest, intermediate, and longest bonds are 2.06 ± 0.02, 2.09 ± 0.02, and 2.11 ± 0.02 Å, respectively. Overall, a mean Co−O bond length of 2.09 ± 0.03 Å is found, with the shortest and longest values equal to 1.975 and 2.204 Å, respectively. Based on the computational results of Varadwaj[35] and Schmiedekamp,[52] three main conclusions can be made. First, the calculations overestimate the Co−O bond lengths by 0.04[35] and 0.06 Å,[52] respectively. Second, unless the geometry is specifically constrained, the distortions in the Co−O bond lengths present in most crystallographically determined structures are not reproduced. Varadwaj et al. have observed a structure with distorted bond lengths; however, it is a fourth-order saddle point. Third, the structure is slightly tilted. This effect is also observed in the solid-state structures: 74% of the structures found in the CSD have complementary angles that differ by more than 4° and nearly 12% have complementary angles differing by more than 10°. Note that Varadwaj[35] performed gas-phase calculations, whereas Schmiedekamp[52] also studied the influence of water as a solvent.

In contrast to the results of Varadwaj and Schmiedekamp, we did not find a stable minimum near to T_h symmetry as negative vibrational frequencies were observed. This is in agreement with the Jahn−Teller (JT) effect, which states that nonlinear molecules with a spatially degenerate electronic ground state undergo a geometrical distortion to lower the energy of the system.[79] Despite the fact that only weak JT effects are expected since the t_{2g} orbitals are unevenly occupied, we observed them in the geometry optimizations. We could identify an optimized structure with D_{2h} symmetry, in which the experimentally observed JT distorted bond lengths are clearly retrieved. The observed bond lengths of the complex with D_{2h} symmetry are 2.03, 2.10, and 2.13 Å. The resulting geometric structure along with the *d*-orbital splitting and atomic contributions is shown in Figure 7(right). This deformed structure is obtained *via* a rhombic distortion, *i.e.*, an unequal amount of elongation or compression along a fourfold axis of rotation. As such, the structure remains orthogonal, but the bond distances are no longer equal. Such JT distorted $[Co(H_2O)_6]^{2+}$ complexes have already been observed by Vlahovic et al.[39] Following the methodology of Zlatar et al., we calculated the JT parameters.[80,81] The results are shown in Table S2. Besides this, we also discovered a structure with S_6 symmetry, acquired *via* a trigonal distortion of the complex, *i.e.*, an elongation/compression along one of the four threefold

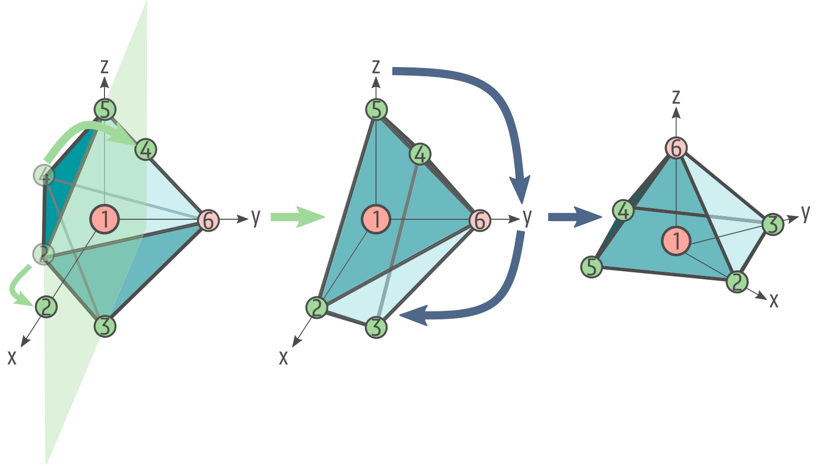

Figure 8. Transformation from a TBP to an SP complex. Ligand positions 2 and 4 are moved until they are situated along the *x*-axis and from together with 3 and 5 a square in the *xz*-plane indicated in green. This is indicated with green arrows. The SP structure is then obtained after a reorientation of the coordinate axes, indicated with blue arrows.

symmetry axes. All ligand bond distances are equal, but the structure is no longer orthogonal. Such distorted complexes have D_{3d} symmetry when the hydrogen atoms are not taken into account. For the complex with S_6 symmetry, all bond lengths are 2.10 Å and the system is tilted at 3.8°. This is shown in Figure 7 (left). This complex is slightly more stable than the complex with D_{2h} symmetry (−10 328 kJ/mol in contrast to −10 311 kJ/mol). The observed point groups along with their symmetry elements are displayed in Figure 6. The coexistence of two different distorted octahedral complexes has already been observed in $K_3[MnF_6]$.[82]

The splitting of the d-orbitals is very similar to the theoretical predictions shown in Figure 3. Some mixing with other contributions different from d-orbitals occurs, which is indicated by dark gray. In general, each MO has a dominant contribution from a specific d-orbital. This can then be used to label the MOs. This is especially the case for the complex with D_{2h} symmetry. The resulting orbitals are shown in Figure S1 and closely resemble those in Figure 4. However, there is more mixing within the t_{2g} and e_g set for the S_6 complex, for which the orbitals are shown in Figure S2. For example, the highest-lying t_{2g} orbital, which contains equal contributions from d_{xy}, d_{xz}, and d_{yz}, differs from the orbitals shown in Figure 4, but the lobes are still oriented in between the coordinated axis. Therefore, the more general label t_{2g} is more convenient. The orbitals in the t_{2g} set are no longer completely degenerate. This is probably due to the presence of contributions different from d-orbitals. This is in agreement with CFT, which reveal that a trigonal distortion splits the t_{2g} but not the e_g orbitals in octahedral complexes.[83] For the D_{2h} complex, also the degeneracy in the e_g set is lifted. The reason for this is that the bonds between the ligands and the metal along the *x*-axis are compressed, resulting in a stronger repulsion between the $d_{x^2-y^2}$ orbital and the metal compared to the d_{z^2} orbital.

The energy difference between the e_g and t_{2g} orbital sets, Δ_o, can be calculated as the difference between the average energy of the e_g and t_{2g} orbitals, being 9065 and 8836 cm^{-1} for the S_6 and D_{2h} structures, respectively. This value is in close agreement with experimental results. Johnson et al.[84] obtained a value of 8400 cm^{-1} starting from experimental absorption spectra *via* the procedure outlined in ref 85. When comparing this value to the mean pairing energy of Co^{2+}, 22 500 cm^{-1}, we indeed see that the HS state is more stable than the LS state.[49,84]

3.3. AOC: $[Co(H_2O)_5]^{2+}$.

As discussed in Section 2, five-coordinated complexes can be TBP or SP, with D_{3h} and C_{4v} symmetry, respectively. For the former, two ligands are oriented along the *z*-axis and the other ligands lie in the *xy*-plane. This configuration can be converted into an SP structure by simple angular distortions, as shown by the green arrows in Figure 8. When the angle between the ligand positions 2 and 4 and the metal center is increased until the ligands lie along the *x*-axis, they form together with 3 and 5 a square in the *xz*-plane indicated with green. As such, the SP structure is obtained, which can easily be recognized after a reorientation of the coordinate axes, indicated with blue arrows in Figure 8. Now, four ligands lie in the *xy*-plane and the remaining ligand is situated along the *z*-axis. The metal center can, but does not have to be in the *xy*-plane. It has been observed that most of the five-coordinated complexes are neither perfectly TBP, nor perfectly SP, but are situated somewhere in between.[53]

When the intrinsic structure of the aqua ligands is taken into account, the most symmetric $[Co(H_2O)_5]^{2+}$ complexes have C_{2v} symmetry, both for the TBP and SP structures. Optimized geometries have been found with C_{2v} and C_1 symmetries, for which the latter is slightly more stable (−8600 kJ/mol in contrast to −8614 kJ/mol). A graphical representation of the symmetry elements and point groups encountered for $[Co(H_2O)_5]^{2+}$ is shown in Figure 9. Structural parameters of the two optimized complexes are listed in Table 2.

We performed continuous shape measurements (CShMs), which evaluate the magnitude of distortion around the metal ion in various complexes,[86,87] to determine whether the complexes are closer to the SP or TBP symmetry. The resulting continuous shape measures (CShMs) for all five possible geometries for five-coordinated structures are given in Table S4, both for the C_{2v} and C_1 complexes. From this, we concluded that the C_{2v} structure is closer to SP, whereas the C_1 structure is closer to TBP. Thus, the TBP complex is a little bit more stable than the SP one. This is in agreement with the literature, where it has been shown that the TBP structure is more stable as there is less ligand−ligand repulsion.[88] However, it has been noted that a distorted SP structure may be only slightly less stable.[88]

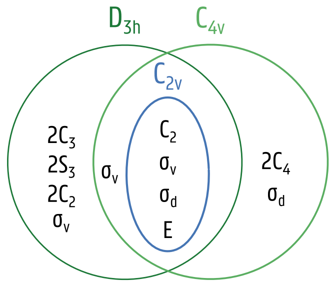

Figure 9. Graphical visualization of the point groups encountered for the five-coordinated complexes, *i.e.*, D_{3h}, C_{4v}, and C_{2v}. All symmetry elements enclosed belong to the corresponding point group.

Table 2. *d*-Orbital Splitting of $[V(H_2O)_6]^{2+}$, $[Mn(H_2O)_6]^{2+}$, and $[Ni(H_2O)_6]^{2+}$ Calculated Using AOC and UDFT[a]

	$[V(H_2O)_6]^{2+}$	$[Mn(H_2O)_6]^{2+}$	$[Ni(H_2O)_6]^{2+}$
AOC	11 883	8104	10 092
UDFT	43 359	8868	52 155
experiment[49]	12 300	7850[b]	8600

[a] The experimental value is also included. [b] Estimated value.

The splitting of the d-orbitals along with the atomic contributions is presented in Figure 10, both for the SP and TBP complexes. Again, each MO has a dominant contribution from a specific d-orbital, which will be used to label the MOs. The orbitals are shown in Figures S3 and S4. In general, the results are in agreement with the theoretical predictions shown in Figure 3, but some differences should be mentioned. The gap between the $d_{x^2-y^2}$ and d_{z^2} orbitals is rather large for the SP complex. Furthermore, d_{xz} and d_{yz} are not completely degenerate. This is not surprising since the complex only has C_{2v} symmetry and not C_{4v}, for which the results are shown in Figure 3. The degeneracy is also lifted for the TBP complex as d_{xz}/d_{yz} and $d_{x^2-y^2}/d_{xy}$ are no longer degenerate.

3.4. AOC: $[Co(H_2O)_4]^{2+}$.

When another ligand is removed, $[Co(H_2O)_4]^{2+}$ complexes are obtained, in which the aqua ligands are situated at the corners of a tetrahedron. When the intrinsic structure of the aqua ligands is taken into account, the most symmetric complexes have D_{2d} symmetry, unlike the T_d symmetry which is found for point-like ligands. In our calculations, the optimized structure does not possess any symmetry. The symmetry elements and point groups encountered for $[Co(H_2O)_4]^{2+}$ are represented graphically in Figure 11. Structural parameters are listed in Table S5.

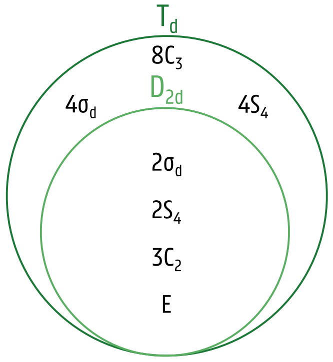

Figure 11. Graphical visualization of the point groups encountered for the four-coordinated complexes, *i.e.*, T_d and D_{2d}. All symmetry elements enclosed belong to the corresponding point group.

The splitting of the d-orbitals and the atomic contributions are shown in Figure 12, and the orbitals are presented in Figure

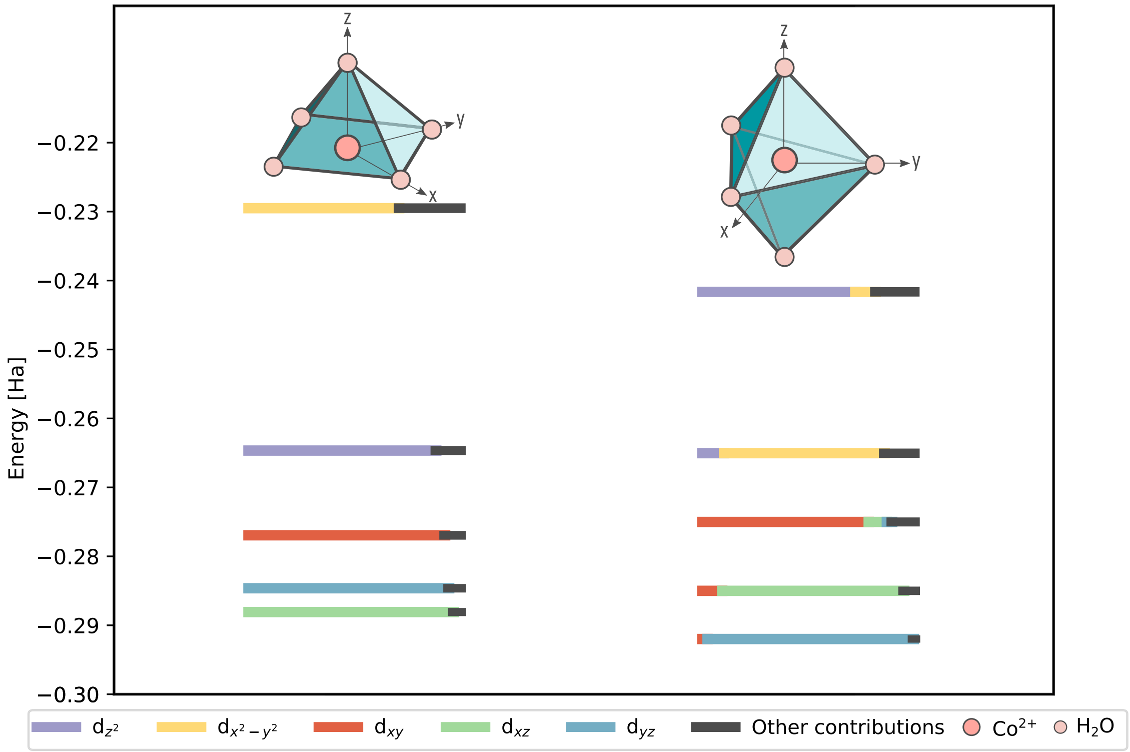

Figure 10. Splitting of the d-orbitals along with their atomic contributions for the optimized $[Co(H_2O)_5]^{2+}$ complexes with C_{2v} symmetry (left) and no symmetry (right).

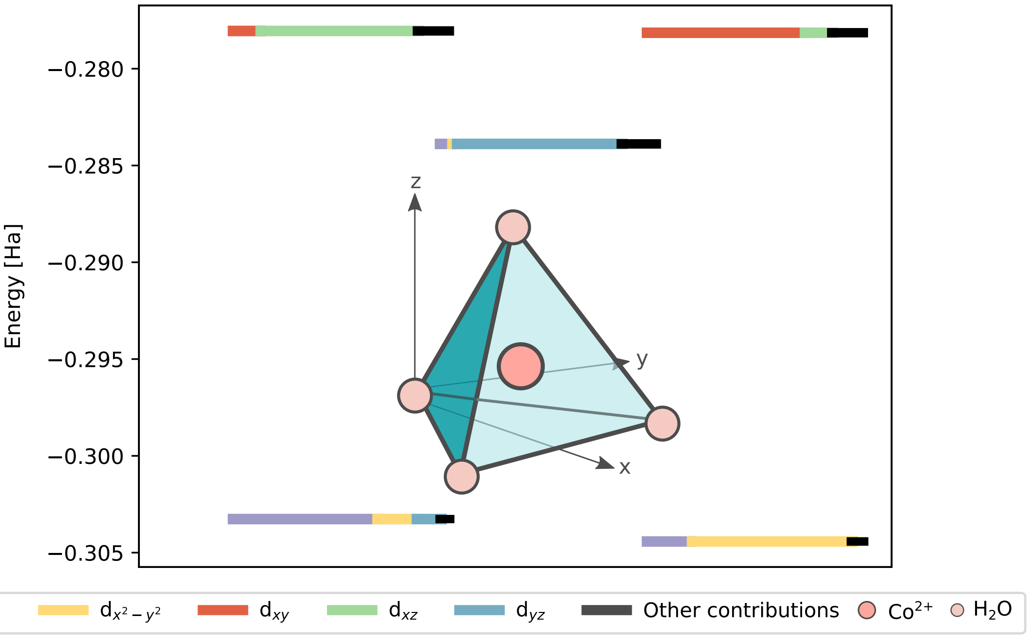

Figure 12. Splitting of the d-orbitals along with their atomic contributions for the optimized $[Co(H_2O)_4]^{2+}$ complex.

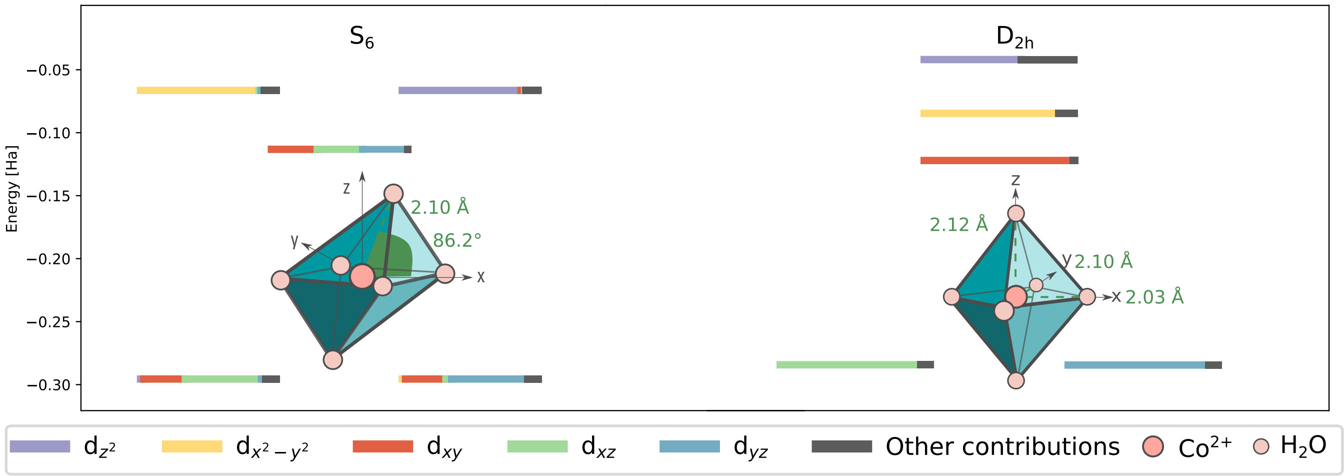

Figure 13. Splitting of the d-orbitals for the optimized $[Co(H_2O)_6]^{2+}$ complexes with S_6 (left) and D_{2h} (right) symmetry calculated by UDFT. Some bond lengths [Å] and bond angles [deg] are also indicated.

S5. The results are in good agreement with these obtained in Figure 3: two orbital sets can be distinguished, t_{2g} and e_g, where the former is less stable than the latter. Due to the fact that the complex is not purely tetrahedral, the degeneracy in the t_{2g} set is lifted slightly. Furthermore, the computed value of Δ_t is 5161 cm^{-1}, which is much smaller than Δ_o, as we expected from AOM.

3.5. Comparison of AOC with UDFT. We compared the AOC results with those from UDFT calculations. The β d-orbital energy levels along with their atomic contributions are shown in Figure 13 for $[Co(H_2O)_6]^{2+}$, as calculated with UDFT. The orbitals are presented in Figures S6 and S7 for completeness. Some major distinctions in comparison with the AOC results need to be highlighted. First of all, we remark that the splitting of the d-orbitals, 50 288 and 53 232 cm^{-1} for S_6 and D_{2h}, respectively, is 1 order of magnitude larger than that for the AOC results and the experimentally found splitting presented in Section 3.2. Second, the t_{2g} set is divided into two low-lying orbitals and one orbital, which is higher in energy. The reason for this is that only two of the β d-orbitals are occupied, resulting in a gap between the highest occupied MO (HOMO) and the lowest unoccupied MO (LUMO).

Additionally, in the UDFT results of the D_{2h} complex, d_{z^2} is higher in energy than $d_{x^2-y^2}$, compared to the AOC results. An explanation for this observation is that UDFT and LFT treat the interelectron repulsion differently, as argued by Deeth et al. for square-planar d^8 Pd complexes.[89] The interelectron repulsion effects are included within a central field approximation in LFT, whereas in UDFT, no central field is assumed and the calculations are performed using the true molecular symmetry of the complex.[89] Therefore, on the one hand, the LFT predictions are in agreement with the AOC results, in which approximate spherical states are constructed by imposing equal fractional occupations. On the other hand, as in the UDFT approach only d_{yz} and d_{xz} are occupied, there is more interelectron repulsion along the z-axis than along the x- or y-axis. Therefore, d_{z^2} will be higher in energy than $d_{x^2-y^2}$. Inspired by the work of Deeth et al., we verified this by

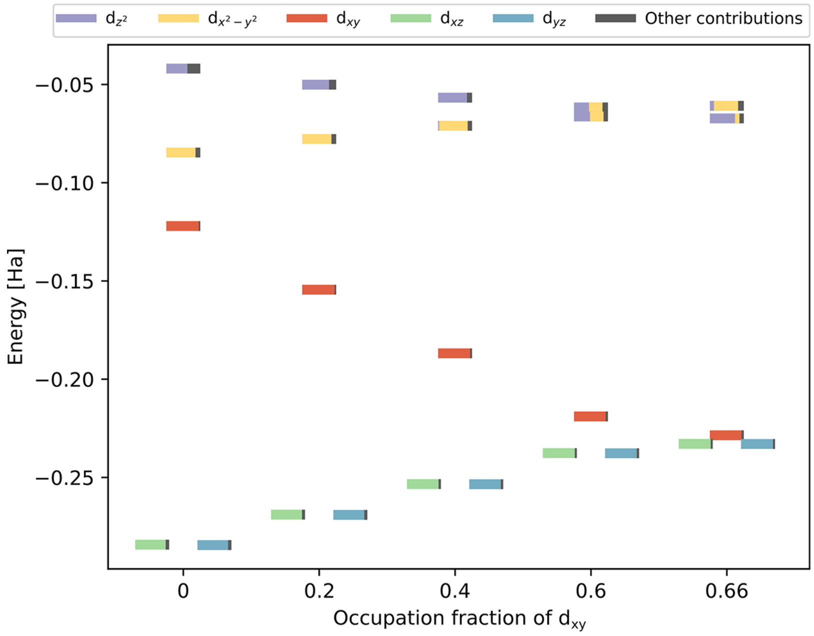

Figure 14. Variation of the splitting of the d-orbitals as a function of the electron occupation fraction of d$_{xy}$ which is transferred equally from d$_{xz}$ and d$_{yz}$ for the $[\mathrm{Co(H_2O)_6}]^{2+}$ complex with D_{2h} symmetry.

systematically removing some portion of the electrons from d$_{xz}$ and d$_{yz}$ and placing it on d$_{xy}$. Therefore, single-point UDFT calculations in which the occupation of the d-orbitals is specified are performed. The results are shown in Figure 14. Two observations can be made as more and more of the electrons initially on d$_{xz}$ and d$_{yz}$ are transferred to d$_{xy}$. First of all, the orbitals become closer in energy and are almost degenerate when 0.66 of an electron is placed at d$_{xy}$. The reason for this is that the two β electrons are now almost equally divided among the three orbitals, resulting in a similar interelectron repulsion along the *x*-, *y*-, and *z*-axes. Second, as more of the electrons is transferred, d$_{z^2}$ and d$_{x^2-y^2}$ increase and decrease in energy, respectively. At an occupation of 0.6 electrons for d$_{xy}$, the two most energetic orbitals presented in Figure 14 have similar contributions of d$_{z^2}$ and d$_{x^2-y^2}$ and are almost degenerate. When *d*$_{xy}$ is populated even more, d$_{x^2-y^2}$ becomes higher in energy than d$_{z^2}$.

In the UDFT results for the S_6 complex, the d$_{x^2-y^2}$ and d$_{z^2}$ orbitals are degenerate just like in the AOC results. Indeed, the effect of the difference in interelectron repulsion is smaller as the two occupied d-orbitals do not only have contributions from d$_{yz}$ and d$_{xz}$ but also from d$_{xy}$. This is shown in Figure S8. As the population of the initially nonoccupied orbital increases, the orbitals with contributions from d$_{xy}$, d$_{xz}$, and d$_{yz}$ become more and more degenerate. However, the energy and contribution of the d$_{x^2-y^2}$ and d$_{z^2}$ orbitals remain similar.

Deviations from the theoretically predicted *d*-orbital splittings are also observed in the five-coordinated complexes as shown in Figure S9. For both SP and TBP, the energy splitting is 1 order of magnitude larger compared to the AOC calculations. Furthermore, in the SP complex, d$_{x^2-y^2}$ and d$_{z^2}$ are interchanged and are almost degenerate. Again, this is due to the different treatment of interelectron repulsion in LFT and UDFT. In the latter, only d$_{xz}$ and d$_{yz}$ are occupied, resulting in more interelectron repulsion along the *z*-axis, therefore d$_{z^2}$ being higher in energy than d$_{x^2-y^2}$. Figure S10 justifies this statement: when d$_{xy}$ is occupied by more than 0.2 electron, d$_{x^2-y^2}$ is higher in energy than d$_{z^2}$. The order of d$_{z^2}$ and d$_{x^2-y^2}$ in the TBP complex is in accordance with the AOC results. Just like for the $[\mathrm{Co(H_2)O_6}]^{2+}$ complex with S_6 symmetry, this is due to the mixed d-orbital contributions of the two lowest occupied MOs. Figure S11 indeed reveals that the orbital energies of the d$_{z^2}$ and d$_{x^2-y^2}$ vary only slightly with the orbital population of d$_{xy}$.

For the four-coordinated complexes, presented in Figure S12, the two lowest β e-orbitals are occupied, and therefore, the splitting is in accordance with the AOC and theoretical results. Nevertheless, the energy gap between the e- and t$_2$-set is still 1 order of magnitude too large.

As stated in ref 89, the observation that UDFT and AOC result in different d-orbitals does not necessarily mean that one of these techniques is right, whereas the other is wrong. Orbitals themselves are not experimentally observable, and therefore, additional properties need to be calculated, like, for example, excited states.[89] The excitations of six-coordinated Co^{2+} aqua-complexes have already been the subject of much research.[36−40] However, to the best of our knowledge, similar studies for five- and four-coordinated complexes are not presented yet.

3.6. $[\mathrm{V(H_2O)_6}]^{2+}$, $[\mathrm{Mn(H_2O)_6}]^{2+}$, and $[\mathrm{Ni(H_2O)_6}]^{2+}$.

To further test the validity of the UDFT calculations, additional calculations have been performed on $[\mathrm{V(H_2O)_6}]^{2+}$, $[\mathrm{Mn(H_2O)_6}]^{2+}$, and $[\mathrm{Ni(H_2O)_6}]^{2+}$, having three, five, and eight d-electrons, respectively. These transition metals have been selected as the t$_{2g}$ set is now completely filled with α electrons for V^{2+} and Mn^{2+} or β electrons for Ni^{2+}. This is in contrast to the partially filled t$_{2g}$ set in $[\mathrm{Co(H_2O)_6}]^{2+}$ containing two β electrons. As such, no JT effects are expected for these systems since the e$_g$ and t$_{2g}$ sets are each evenly occupied. This is also observed from the calculations for the V^{2+} and Ni^{2+} complexes as stable complexes with T_h symmetry are retrieved. However, this is not the case for the Mn^{2+} complex, for which the most symmetric stable complexes have S_6 and D_{2h} symmetries. Systems with S_6 and D_{2h} symmetries have also been obtained for V^{2+} and Ni^{2+}. All structures have, within 3 kJ/mol, the same energy and we will show and discuss the results for the

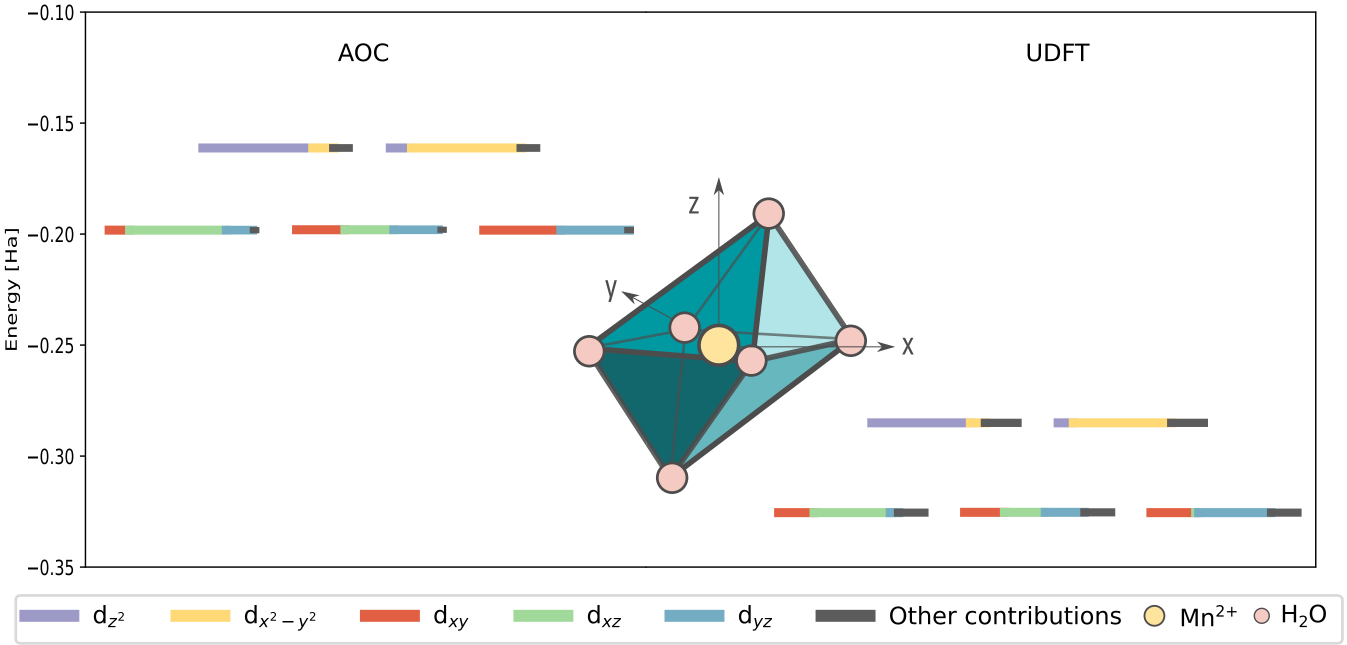

Figure 15. Splitting of the d-orbitals for the optimized $[Mn(H_2O)_6]^{2+}$ complexes with S_6 symmetry using AOC (left) and UDFT (right).

complexes with S_6 symmetry. The d-orbital splittings along with the atomic contributions are shown in Figures 15, S13, and S14 for $[Mn(H_2O)_6]^{2+}$, $[V(H_2O)_6]^{2+}$, and $[Ni(H_2O)_6]^{2+}$, respectively. For Mn^{2+} and V^{2+}, the α-electrons are shown for the UDFT calculations, whereas the β-electrons are presented for Ni^{2+}. The reason for this is that the spin-allowed d−d transitions will be within α/β-electrons for V^{2+}/Ni^{2+}, respectively. For Mn^{2+}, there are no spin-allowed d−d transitions. First, remark that, for all of the systems, both AOC and UDFT correctly predict the splitting into a t_{2g} and e_g set, which is in agreement with the qualitative LFT results. This is due to the fact that for these systems, the t_{2g} orbitals are either completely filled with α-electrons, as is the case for Mn^{2+} and V^{2+}, or with both α- and β-electrons, as is the case for the Ni^{2+} complex. Second, for $[Mn(H_2O)_6]^{2+}$, all α-d-orbitals are occupied, which results in a correct prediction of the magnitude of the d-orbital splitting by both AOC and UDFT. This result is not surprising since the only differences between the AOC and UDFT calculations are due to the spin polarization which is absent in the former. However, as is the case for the Co^{2+} complex, the splitting is severely overestimated by UDFT for $[V(H_2O)_6]^{2+}$ and $[Ni(H_2O)_6]^{2+}$. This is also shown in Table 2 in which the d-orbital splitting obtained from experiment,[49] AOC, and UDFT calculations is presented for the various complexes. This observation is in agreement with ref 89, in which it was argued that DFT is expected to yield the same *d*-orbitals sequence as LFT in those cases where a suitable spherical configuration is constructed corresponding to equal populations of the d-orbitals as for d^{10} or HS d^5 complexes. Here, this observation is confirmed and extended to octahedral d^3, d^5, and d^8 systems.

4. CONCLUSIONS

In this work, we investigated Co^{2+} aqua-complexes with six, five, and four ligands. The ground-state properties have been examined, and a lot of attention has been paid to the electronic structure. More specifically, we focused on the energy splitting of the d-electrons and how this depends on the symmetry, where both the influence on the coordination environment and the specific point group are considered. Qualitative techniques such as CFT and LFT reveal that the d-orbital splitting is characteristic of the number of ligands coordinated to the TM. To obtain quantitative results, DFT calculations have been performed, both AOC and UDFT. Stable Co^{2+} aqua-complexes with six, five, and four ligands have been obtained from UDFT optimizations. We have observed a stable structure containing six aqua ligands with D_{2h} symmetry in which JT distortions are clearly visible. Besides this, we also found a structure with S_6 symmetry. Moreover, we have shown that the AOC method is capable of reproducing the d-orbital splittings obtained from the qualitative techniques. UDFT calculations do not succeed in this when only part of the d-orbitals are occupied. Indeed, the energy gap between the d-orbitals and the energy difference between the HOMO and LUMO are overestimated by UDFT for six-coordinated aqua-complexes. As such, the t_{2g} orbitals are far from degenerate as we would expect based on qualitative techniques. Based on the work of Deeth et al., we demonstrated that the discrepancies between UDFT and AOC are due to the different electron occupations resulting in different interelectron repulsions. The AOC orbitals confirm the chemical intuition as given by LFT as both techniques describe the electron repulsion in a spherical way, which was also shown by Daul et al.[47] The d-orbital splitting obtained by UDFT will be different due to the integer occupation numbers resulting in different interelectron repulsions. To further test the performance of UDFT, other TMs have been investigated. We selected TMs for which the t_{2g} set is occupied evenly. The results for these systems are qualitatively in agreement with for example LFT. Furthermore, for $[Mn(H_2O)_6]^{2+}$, for which all α d-orbitals are occupied, even the d-orbital splitting is described correctly and in agreement with the AOC calculations and experimental results. The proper understanding of the electronic structure and symmetry of TMCs is a key element for obtaining insights into the formation process of MOFs and potentially also their defect structures.

■ ASSOCIATED CONTENT

Supporting Information

The Supporting Information is available free of charge at https://pubs.acs.org/doi/10.1021/acs.inorgchem.2c02358.

> Extra computational details, visualization of the orbitals, structural information, CShMs for the $[Co(H_2O)_6]^{2+}$ complexes, additional splittings of the d-orbitals, and geometries of optimized structures (PDF)

■ AUTHOR INFORMATION

Corresponding Author

Veronique Van Speybroeck − *Center for Molecular Modeling (CMM), Ghent University, 9052 Zwijnaarde, Belgium;* orcid.org/0000-0003-2206-178X; Email: Veronique.VanSpeybroeck@UGent.be

Author

Liesbeth De Bruecker − *Center for Molecular Modeling (CMM), Ghent University, 9052 Zwijnaarde, Belgium;* orcid.org/0000-0001-7844-6932

Complete contact information is available at: https://pubs.acs.org/10.1021/acs.inorgchem.2c02358

Notes

The authors declare no competing financial interest.

■ ACKNOWLEDGMENTS

The authors acknowledge the Research Board of Ghent University (BOF) for funding. The computational resources and services used in this work were provided by VSC (Flemish Supercomputer Center), funded by Ghent University, FWO, and the Flemish Government Department EWI.

■ REFERENCES

(1) Park, K. S.; Ni, Z.; Côté, A. P.; Choi, J. Y.; Huang, R.; Uribe-Romo, F. J.; Chae, H. K.; O'Keeffe, M.; Yaghi, O. M. Exceptional Chemical and Thermal Stability of Zeolitic Imidazolate Frameworks. *Proc. Natl. Acad. Sci. U.S.A.* **2006**, *103*, 10186−10191.

(2) Öztürk, Z.; Hofmann, J. P.; Lutz, M.; Mazaj, M.; Logar, N. Z.; Weckhuysen, B. M. Controlled Synthesis of Phase-Pure Zeolitic Imidazolate Framework Co-ZIF-9. *Eur. J. Inorg. Chem.* **2015**, *2015*, 1625−1630.

(3) Cravillon, J.; Schröder, C. A.; Bux, H.; Rothkirch, A.; Caro, J.; Wiebcke, M. Formate Modulated Solvothermal Synthesis of ZIF-8 Investigated using Time-Resolved in Situ X-Ray Diffraction and Scanning Electron Microscopy. *CrystEngComm* **2012**, *14*, 492−498.

(4) Cravillon, J.; Nayuk, R.; Springer, S.; Feldhoff, A.; Huber, K.; Wiebcke, M. Controlling Zeolitic Imidazolate Framework Nano- and Microcrystal Formation: Insight into Crystal Growth by Time-Resolved In Situ Static Light Scattering. *Chem. Mater.* **2011**, *23*, 2130−2141.

(5) Cravillon, J.; Menzer, S.; Lohmeier, S.-J.; Feldhoff, A.; Huber, K.; Wiebcke, M. Rapid Room-Temperature Synthesis and Characterization of Nanocrystals of a Prototypical Zeolitic Imidazolate Framework. *Chem. Mater.* **2009**, *21*, 1410−1412.

(6) Cravillon, J.; Schröder, C. A.; Nayuk, R.; Gummel, J.; Huber, K.; Wiebcke, M. Fast Nucleation and Growth of ZIF-8 Nanocrystals Monitored by Time-Resolved In Situ Small-Angle and Wide-Angle X-Ray Scattering. *Angew. Chem.* **2011**, *123*, 8217−8221.

(7) Venna, S. R.; Jasinski, J. B.; Carreon, M. A. Structural Evolution of Zeolitic Imidazolate Framework-8. *J. Am. Chem. Soc.* **2010**, *132*, 18030−18033.

(8) Phan, A.; Doonan, C. J.; Uribe-Romo, F. J.; Knobler, C. B.; O'Keeffe, M.; Yaghi, O. M. Synthesis, Structure, and Carbon Dioxide Capture Properties of Zeolitic Imidazolate Frameworks. *Acc. Chem. Res.* **2010**, *43*, 58−67.

(9) Hayashi, H.; Côté, A. P.; Furukawa, H.; O'Keeffe, M.; Yaghi, O. M. Zeolite A Imidazolate Frameworks. *Nat. Mater.* **2007**, *6*, 501−506.

(10) Fedorchuk, C.; Swaddle, T. W. Comment on Reinterpretation of the Spectra of Hydrated Co^{++}: An ab Initio Study (J. Phys. Chem. A 1998, 102, 6525). *J. Phys. Chem. A* **2000**, *104*, 5651−5652.

(11) Yao, J.; Wang, H. Zeolitic Imidazolate Framework Composite Membranes and Thin Films: Synthesis and Applications. *Chem. Soc. Rev.* **2014**, *43*, 4470−4493.

(12) Sun, Y.; Rogge, S. M. J.; Lamaire, A.; Vandenbrande, S.; Wieme, J.; Siviour, C. R.; Speybroeck, V. V.; Tan, J.-C. High-Rate Nanofluidic Energy Absorption in Porous Zeolitic Frameworks. *Nat. Mater.* **2021**, *20*, 1015−1023.

(13) Hu, Y.; Kazemian, H.; Rohani, S.; Huang, Y.; Song, Y. In Situ High Pressure Study of ZIF-8 by FTIR Spectroscopy. *Chem. Commun.* **2011**, *47*, 12694−12696.

(14) Sun, C.-Y.; Qin, C.; Wang, X.-L.; Yang, G.-S.; Shao, K.-Z.; Lan, Y.-Q.; Su, Z.-M.; Huang, P.; Wang, C.-G.; Wang, E.-B. Zeolitic Imidazolate Framework-8 as Efficient pH-Sensitive Drug Delivery Vehicle. *Dalton Trans.* **2012**, *41*, 6906−6909.

(15) Moggach, S. A.; Bennett, T. D.; Cheetham, A. K. The Effect of Pressure on ZIF-8: Increasing Pore Size with Pressure and the Formation of a High-Pressure Phase at 1.47GPa. *Angew. Chem., Int. Ed.* **2009**, *48*, 7087−7089.

(16) Kaur, G.; Rai, R. K.; Tyagi, D.; Yao, X.; Li, P.-Z.; Yang, X.-C.; Zhao, Y.; Xu, Q.; Singh, S. K. Room-Temperature Synthesis of Bimetallic CoZn Based Zeolitic Imidazolate Frameworks in Water for Enhanced CO_2 and H_2 Uptakes. *J. Mater. Chem. A* **2016**, *4*, 14932−14938.

(17) Kwon, H. T.; Jeong, H.-K.; Lee, A. S.; An, H. S.; Lee, J. S. Heteroepitaxially Grown Zeolitic Imidazolate Framework Membranes with Unprecedented Propylene/Propane Separation Performances. *J. Am. Chem. Soc.* **2015**, *137*, 12304−12311.

(18) Wang, C.; Yang, F.; Sheng, L.; Yu, J.; Yao, K.; Zhang, L.; Pan, Y. Synthesis of Isoalkanes over a Core (FeZnZr)Shell (Zeolite) Catalyst by CO_2 Hydrogenation. *Chem. Commun.* **2016**, *52*, 12578−12581.

(19) Yang, H.; He, X.-W.; Wang, F.; Kang, Y.; Zhang, J. Doping Copper into ZIF-67 for Enhancing Gas Uptake Capacity and Visible-Light-Driven Photocatalytic Degradation of Organic Dye. *J. Mater. Chem.* **2012**, *22*, 21849−21851.

(20) Lee, Y.-R.; Jang, M.-S.; Cho, H.-Y.; Kwon, H.-J.; Kim, S.; Ahn, W.-S. ZIF-8: AComparison of Synthesis Methods. *Chem. Eng. J.* **2015**, *271*, 276−280.

(21) Banerjee, R.; Phan, A.; Wang, B.; Knobler, C.; Furkawa, H.; O'Keeffe, M.; Yaghi, O. M. High-Throughput Synthesis of Zeolitic Imidazolate Frameworks and Application to CO2 Capture. *Science* **2008**, *319*, 939−943.

(22) Van Vleet, M. J.; Weng, T.; Li, X.; Schmidt, J. R. In Situ, Time-Resolved, and Mechanistic Studies of Metal-Organic Framework Nucleation and Growth. *Chem. Rev.* **2018**, *118*, 3681−3721.

(23) Rimer, J. D.; Tsapatsis, M. Nucleation of Open Framework Materials: Navigating the Voids. *MRS Bull.* **2016**, *41*, 393−398.

(24) Filez, M.; Caratelli, C.; Rivera-Torrente, M.; Muniz-Miranda, F.; Hoek, M.; Altelaar, M.; Heck, A. J. R.; Speybroeck, V. V.; Weckhuysen, B. M. Elucidation of the Pre-Nucleation Phase Directing Metal-Organic Framework Formation. *Cell Rep. Phys. Sci.* **2021**, *2*, No. 100680.

(25) Barone, V.; Alessandrini, S.; Biczysko, M.; Cheeseman, J. R.; Clary, D. C.; McCoy, A. B.; DiRisio, R. J.; Neese, F.; Melosso, M.; Puzzarini, C. Computational Molecular Spectroscopy. *Nat. Rev. Methods Primers* **2021**, *1*, No. 38.

(26) Stepanović, S.; Zlatar, M.; Swart, M.; Gruden, M. The Irony of Manganocene: An Interplay between the JahnTeller Effect and Close-Lying Electronic and Spin States. *J. Chem. Inf. Model.* **2019**, *59*, 1806−1810.

(27) Flöser, B. M.; Guo, Y.; Riplinger, C.; Tuczek, F.; Neese, F. Detailed Pair Natural Orbital-Based Coupled Cluster Studies of Spin Crossover Energetics. *J. Chem. Theory Comput.* **2020**, *16*, 2224−2235.

(28) Stavila, V.; Bulimestru, I.; Gulea, A.; Colson, A. C.; Whitmire, K. H. Hexaaquacobalt(II) and Hexaaquanickel(II) bis(μ-pyridine-2,6-dicarboxylato)bis[(pyridine-2,6-dicarboxyl- ato)bismuthate(III)] dihydrate. *Acta Crystallogr., Sect. C: Cryst. Struct. Commun.* **2011**, *67*, m65−m68.

(29) Jørgensen, C. K.; de Verdier, C. H.; Glomset, J.; et al. Studies of Absorption Spectra. IV. Some New Transition Group BAnds of Low Intensity. *Acta Chem. Scand.* **1954**, *8*, 1502−1512.

(30) Holmes, O. G.; McClure, D. S. Optical Spectra of Hydrated Ions of the Transition Metals. *J. Chem. Phys.* **1957**, *26*, 1686.

(31) Jörgensen, C. K.*Spectroscopy of Transition-Group Complexes in Advances in Chemical Physics*; John Wiley and Sons, Inc., 1963.

(32) Jörgensen, C. K.*Absorption Spectra and Chemical Bonding in Complexes*; Pergamon Press, 1962.

(33) Griffith, J. S.*The Theory of Transition-Metal Ions*; Cambridge University Press, 1964.

(34) Spezia, R.; Tournois, G.; Tortajada, J.; Cartailler, T.; Gaigeot, M.-P. Toward a DFT-Based Molecular Dynamics Description of Co(II) Binding in Sulfur-Rich Peptide. *Phys. Chem. Chem. Phys.* **2006**, *8*, 2040−2050.

(35) Varadwaj, P. R.; Marques, H. M. The Physical Chemistry of Coordinated Aqua-, Ammine-, and Mixed-Ligand Co^{2+} Complexes: DFT Studies on the Structure, Energetics, and Topological Properties of the Electron Density. *Phys. Chem. Chem. Phys.* **2010**, *12*, 2126−2138.

(36) Neese, F.; Petrenko, T.; Ganyushin, D.; Olbrich, G. Advanced Aspects of Ab Initio Theoretical Optical Spectroscopy of Transition Metal Complexes: Multiplets, Spin-Orbit Coupling and Resonance Raman Intensities. *Coord. Chem. Rev.* **2007**, *251*, 288−327.

(37) Boeyens, J. C. A.; Ogilvie, J. F.*Models, Mysteries and Magic of Molecules*; Springer, 2008.

(38) Yang, Y.; Ratner, M. A.; Schatz, G. C. Multireference Ab Initio Study of Ligand Field dd Transitions in Octahedral Transition-Metal Oxide Clusters. *J. Phys. Chem. C* **2014**, *118*, 29196−29208.

(39) Vlahović, F.; Peric, M.; Gruden-Pavlović, M.; Zlatar, M. Assessment of TD-DFT and LF-DFT for Study of d-d Transitions in First Row Transition Metal Hexaaqua Complexes. *J. Chem. Phys.* **2015**, *142*, No. 214111.

(40) Radoń, M.; Drabik, G. Spin States and Other Ligand-Field States of Aqua Complexes Revisited with Multireference ab Initio Calculations Including Solvation Effects. *J. Chem. Theory Comput.* **2018**, *14*, 4010−4027.

(41) Bethe, H. Termaufspaltung in Kristallen. *Ann. Phys.* **1929**, *395*, 133−208.

(42) Van Vleck, J. H. Theory of the Variations in Paramagnetic Anisotropy Among Different Salts of the Iron Group. *Phys. Rev.* **1932**, *41*, 208−215.

(43) Van Vleck, J. H. Valence Strength and the Magnetism of Complex Salts. *J. Chem. Phys.* **1935**, *3*, 807−813.

(44) Griffith, J. S.; Orgel, L. E. Ligand-Field Theory. *Q. Rev. Chem. Soc.* **1957**, *11*, 381−393.

(45) Larsen, E.; La Mar, G. N. The Angular Overlap Model: How to use it and why. *J. Chem. Educ.* **1974**, *51*, 633−640.

(46) Burdett, J. K.*Molecular Shapes*; John Wiley & Sons, Inc., 1980.

(47) Atanasov, M.; Daul, C. A.; Rauzy, C. A DFT Based Ligand Field Theory. *Struct. Bonding* **2004**, *106*, 97−125.

(48) Ciampolini, M.*Spectra of 3d Five-Coordinate Complexes*; Springer, 1969.

(49) Miessler, G. L.; Fischer, P. J.; Tarr, D. A.*Inorganic Chemistry*; Pearson, 2014.

(50) Solomon, E. I.; Pavel, E. G.; Loeb, K. E.; Campochiaro, C. Magnetic Circular Dichroism Spectroscopy as a Probe of the Geometric and Electronic Structure of Non-Heine Ferrous Enzymes. *Coord. Chem. Rev.* **1995**, *114*, 369−460.

(51) Shriver, D. F.; Langford, C. H.; Atkins, P. W.*Inorganic Chemistry*; H. Freeman and Co., 1994.

(52) Schmiedekamp, A. M.; Ryan, M. D.; Deeth, R. J. Six-Coordinate Co^{2+} with H_2O and NH_3 Ligands: Which Spin State Is More Stable? *Inorg. Chem.* **2002**, *41*, 5733−5743.

(53) Sacconi, L. Five-Coordination in 3d Complexes. *Pure Appl. Chem.* **1968**, *17*, 95−128.

(54) Sacconi, L. Some Factors Governing the Spin-Multiplicity of 5-Coordinate Complexes of Cobalt(II) and Nickel(II). *J. Chem. Soc. A* **1970**, 248−256.

(55) Slater, J. C.*The Self-Consistent Field for Molecules and Solids*; McGraw-Hill: New York, 1974.

(56) te Velde, G.; Bickelhaupt, F. M.; Baerends, E.; Guerra, C. F.; van Gisbergen, S.; Snijders, J.; Ziegler, T. Chemistry with ADF. *J. Comput. Chem.* **2001**, *22*, 931−967.

(57) Pye, C. C.; Ziegler, T. An Implementation of the Conductor-Like Screening Model of Solvation Within the Amsterdam Density Functional Package. *Ther. Chem. Acc.* **1999**, *101*, 396−408.

(58) Lenthe, E. v.; Baerends, E. J.; Snijders, J. G. Relativistic Regular Two-Component Hamiltonians. *J. Chem. Phys.* **1993**, *99*, 4597.

(59) van Lenthe, E.; Baerends, E. J.; Snijders, J. G. Relativistic total energy using regular approximations. *J. Chem. Phys.* **1994**, *101*, 9783−9792.

(60) van Lenthe, E.; Ehlers, A.; Baerends, E. J. Geometry Optimization in the Zero Order Regular Approximation for Relativistic Effects. *J. Chem. Phys.* **1999**, *110*, 8943−8953.

(61) Grimme, S.; Antony, J.; Ehrlich, S.; Krieg, H. A Consistent and Accurate Ab Initio Parametrization of Density Functional Dispersion Correction (DFT-D) for the 94 Elements H-Pu. *J. Chem. Phys.* **2010**, *132*, No. 154104.

(62) Lee, C.; Yang, W.; Parr, R. G. Development of the Colle-Salvetti Correlation-Energy Formula into a Functional of the Electron Density. *Phys. Rev. B* **1988**, *37*, 785.

(63) Becke, A. D. Density-functional exchange-energy approximation with correct asymptotic behavior. *Phys. Rev. A* **1988**, *38*, 3098−3100.

(64) Zhao, Y.; Truhlar, D. G. A New Local Density Functional for Main-Group Thermochemistry, Transition Metal Bonding, Thermochemical Kinetics, and Noncovalent Interactions. *J. Chem. Phys.* **2006**, *125*, No. 194101.

(65) Yu, H. S.; He, X.; Truhlar, D. G. MN15-L: ANew Local Exchange-Correlation Functional for KohnSham Density Functional Theory with Broad Accuracy for Atoms, Molecules, and Solids. *J. Chem. Theory Comput.* **2016**, *12*, 1280−1293.

(66) Cohen, A. J.; Handy, N. C. Dynamic Correlation. *Mol. Phys.* **2001**, *99*, 607−615.

(67) Becke, A. D. DensityFunctional Thermochemistry. III. The Role of Exact Exchange. *J. Chem. Phys.* **1993**, *98*, 5648.

(68) Xu, X.; Goddard, W. A., III. The X3LYP Extended Density Functional for Accurate Descriptions of Nonbond Interactions, Spin States, and Thermochemical Properties. *Proc. Natl. Acad. Sci. U.S.A.* **2004**, *101*, 2673−2677.

(69) Adamo, C.; Barone, V. Toward Reliable Density Functional Methods Without Adjustable Parameters: The PBE0 Model. *J. Chem. Phys.* **1999**, *110*, 6158−6169.

(70) Yu, H. S.; He, X.; Li, S. L.; Truhlar, D. G. MN15: A Kohn-Sham Global-Hybrid Exchange-Correlation Density Functional with Broad Accuracy for Multi-Reference and Single-Reference Systems and Noncovalent Interactions. *Chem. Sci.* **2016**, *7*, 5032−5051.

(71) Staroverov, V. N.; Scuseria, G. E.; Tao, J.; Perdew, J. P. Comparative Assessment of a New Nonempirical Density Functional: Molecules and Hydrogen-Bonded Complexes. *J. Chem. Phys.* **2003**, *119*, 12129−12137.

(72) Tao, J.; Perdew, J. P.; Staroverov, V. N.; Scuseria, G. E. Climbing the Density Functional Ladder: Nonempirical Meta-Generalized Gradient Approximation Designed for Molecules and Solids. *Phys. Rev. Lett.* **2003**, *91*, No. 146401.

(73) Yanai, T.; Tew, D. P.; Handy, N. C. A New Hybrid Exchange-Correlation Functional using the Coulomb-Attenuating Method (CAM-B3LYP). *Chem. Phys. Lett.* **2004**, *393*, 51−57.

(74) Chai, J.-D.; Head-Gordon, M. Long-Range Corrected Hybrid Density Functionals with Damped AtomAtom Dispersion Corrections. *Phys. Chem. Chem. Phys.* **2008**, *10*, 6615−6620.

https://doi.org/10.1021/acs.inorgchem.2c02358
Inorg. Chem. 2022, 61, 20743−20756

(75) Dennington, R.; Keith, T. A.; Millam, J. M.*GaussView*, version 5; Semichem Inc.: Shawnee Mission, KS, 2019.

(76) Shee, J.; Loipersberger, M.; Hait, D.; Lee, J.; Head-Gordon, M. Revealing the Nature of Electron Correlation in Transition Metal Complexes with Symmetry-Breaking and Chemical Intuition. *J. Chem. Phys.* **2021**, *154*, No. 194109.

(77) Neese, F.; Ames, W.; Christian, G.; Kampa, M.; Liakos, D. G.; Pantazis, D. A.; Roemelt, M.; Surawatanawong, P.; Ye, S.Dealing with Complexity in Open-shell Transition Metal Chemistry from a Theoretical Perspective: Rection Pathways, Bonding, Spectroscopy, and Magnetic Properties. *Advances in Inorganic Chemistry*; Elsevier Inc., 2010.

(78) CSD Cambridge UK. *Cambridge Structural Database*, v.5.30; CSD Cambridge, 2008 (updated to Sept 2009).

(79) Jahn, H. A.; Teller, E. Stability of Polyatomic Molecules in Degenerate Electronic States. I. Orbital Degeneracy. *Proc. R. Soc. London, Ser. A* **1937**, *161*, 220−235.

(80) Zlatar, M.; Schläpfer, C.-W.; Daul, C.*A New Method to Describe the Multimode Jahn−Teller Effect Using Density Functional Theory*; Springer, 2009.

(81) Kundu, T. K.; Bruyndonckx, R.; Daul, C.; Manoharan, P. T. A Density Functional Approach to the Jahn-Teller Effect of $[Cu(en)_3]^{2+}$ as a Model for a Macrobicyclic Cage Complex of Copper(ii). *Inorg. Chem.* **1999**, *38*, 3931−3934.

(82) Stoll, C.; Atanasov, M.; Bandemehr, J.; Neese, F.; Pietzonka, C.; Kraus, F.; Karttunen, A. J.; Heymann, G.; Seibald, M.; Huppertz, H. Coexistence of Two Different Distorted Octahedral $[MnF_6]^{3-}$ Sites in $K_3[MnF_6]$: Manifestation in Spectroscopy and Magnetism. *Chem.—Eur. J.* **2021**, *27*, 9801−9813.

(83) Figgis, B. N.; Hitchman, M. A.*Ligand Fielt Theory and Its Applications*; Wiley, 2000.

(84) Johnson, D. A.; Nelson, P. G. Factors Determining the Ligand Field Stabilization Energies of the Hexaaqua 2+ Complexes of the First Transition Series and the Irving-Williams Order. *Inorg. Chem.* **1995**, *34*, 5666−5671.

(85) Reedijk, J.; Driessen, W. L.; Groeneveld, W. L. A Semi-Empirical Energy-Level Diagram for Octahedral Cobalt(II) Complexes. *Recl. Trav. Chim. Pays-Bas* **2010**, *88*, 1095−1109.

(86) Hargittai, I. Book Review: Fuzzy Definitions: Concepts in Chemistry—A Contemporary Challenge. Edited by D. H. Rouvray. *Angew. Chem., Int. Ed.* **1997**, *36*, 2525.

(87) Zabrodsky, H.; Peleg, S.; Avnir, D. Continuous Symmetry Measures. *J. Am. Chem. Soc.* **1992**, *114*, 7843−7851.

(88) Zemann, J. Elektrostatische Energien von AB_5-Komplexen. *Z. Anorg. Allg. Chem.* **1963**, *324*, 241−249.

(89) Deeth, R. J. Ligand Field and Density Functional Descriptions of the d-States and Bonding in Transition Metal Complexes. *Faraday Discuss.* **2003**, *124*, 379−391.